

Simulating the mass-metallicity relation from $z \sim 1^*$

M. Mouhcine¹, B. K. Gibson^{2,3}, A. Renda⁴, and D. Kawata^{4,5}

¹ Astrophysics Research Institute, Liverpool John Moores University, Twelve Quays House, Egerton Wharf, Birkenhead, CH41 1LD, UK

² Centre for Astrophysics, University of Central Lancashire, Preston, PR1 2HE, UK

³ School of Physics, University of Sydney, NSW, 2006, Australia

⁴ Centre for Astrophysics & Supercomputing, Swinburne University, Hawthorn, Victoria, 3122, Australia

⁵ The Observatories of the Carnegie Institution of Washington, 813 Santa Barbara Street, Pasadena, CA, 91101 USA

Preprint online version: November 18, 2018

ABSTRACT

Context. The chemical properties of galaxies and their evolution as a function of cosmic epoch are powerful constraints of their evolutionary histories.

Aims. This work provides a grid of numerical models of galaxy evolution over an extended cosmic epoch. The aims are to assess how well current models reproduce observed properties of galaxies, in particular the stellar mass versus gas phase metallicity relation, and to quantify the effect of the merging histories of galaxies on their final properties.

Methods. We use 112 N-body/hydrodynamical simulations in the standard Cold Dark Matter universe, to follow the formation of galaxy-sized halos and investigate the chemical enrichment of both the stellar component and the interstellar medium of galaxies, with stellar masses larger than $\sim 10^9 M_\odot$.

Results. The resulting chemical properties of the simulated galaxies are broadly consistent with the observations. The predicted relationship between the mean metallicity and the galaxy stellar mass for both the stellar and the gaseous components at $z = 0$ are in agreement with the relationships observed locally. The predicted scatter about these relationships, which is traced to the differing merging histories amongst the simulated galaxies with similar final masses, is similar to that observed. Under the hierarchical formation scenario, we find that the more massive galaxies are typically more evolved than their low mass counterparts over the second half of the age of the Universe. The predicted correlations between the total mass and the stellar mass of galaxies in our simulated sample from the present epoch up to $z \sim 1$ agree with observed ones. We find that the integrated stellar populations in the simulations are dominated by stars as old as 4 – 10 Gyr. In contrast with massive galaxies, for which the luminosity-weighted ages of the integrated stellar populations in the simulated sample agree with those derived from the modeling of observed spectral energy distributions, simulated galaxies with stellar masses $\sim 10^9 M_\odot$ at $z = 0$ tend to be older than the local galaxies with similar stellar masses.

Conclusions. The stellar mass versus metallicity relation and its associated scatter are reproduced by the simulations as consequences of the increasing efficiency of the conversion of gas into stars with stellar mass, and the differing merging histories amongst the galaxies with similar masses. The old ages of simulated low mass galaxies at $z = 0$, and the weak level of chemical evolution for massive galaxies suggest however that our modelling of the supernova feedback may be incomplete, or that other feedback processes have been neglected.

Key words. Methods: numerical – Galaxies: abundances – Galaxies: evolution – Galaxies: formation

1. Introduction

The chemical enrichment histories of galaxies provide insight into various processes involved in galaxy formation and evolution. The chemical composition of stars and gas within a galaxy depends on a number of physical processes, such as the star formation history, gas outflows and inflows, stellar initial mass function, etc. Although it is a

complicated task to disentangle the effects of these processes, the galactic chemical abundances at various epochs place tight constraints on the likely evolutionary histories of galaxies.

The correlation between galaxy metallicity and luminosity in the local universe is one of the most significant observational results in galaxy chemical evolution studies. Lequeux et al. (1979) first revealed that the oxygen abundance increases with the total mass of irregular galaxies. The luminosity-metallicity relation for ir-

* Research undertaken as part of the Commonwealth Cosmology Initiative (CCI:www.thecci.org).

regulars was later confirmed by Skillman et al. (1989) and Richer & McCall (1995), amongst others. Subsequent studies have extended the relation to spiral galaxies (e.g., Garnett & Shields 1987; Zaritsky et al. 1994; Garnett et al. 1997; Pilyugin & Ferrini 2000), and to elliptical galaxies (Brodie & Huchra 1991). The luminosity correlates with metallicity over ~ 10 magnitudes in luminosity and a factor of ~ 100 in metallicity, with indications suggesting that the relationship may be independent of environment (Vilchez 1995; Mouhcine et al. 2007) and morphology (Mateo 1998). More recently, large samples of star-forming galaxies drawn from galaxy redshift surveys, e.g. 2dF Galaxy Redshift Survey and the Sloan Digital Sky Survey (SDSS hereafter), have been used to confirm the existence of the luminosity-metallicity relation over a broad range of luminosity and metallicity (Lamareille et al. 2004; Tremonti et al. 2004). Lee et al. (2006) have extended the mass-metallicity relation to dwarf irregular galaxies, and found that the dispersion is similar over five orders of magnitude in stellar mass, and that the relation between the integrated stellar mass and the oxygen abundance of the interstellar medium is similarly tight from high stellar mass to low stellar mass galaxies. **The gas phase oxygen abundance vs. stellar mass has been understood either as a depletion sequence or a sequence in astration (see e.g. Tremonti et al. 2004). Köppen, Weidner, & Kroupa (2007) have presented an alternative explanation of the mass-metallicity relation arguing it could be the consequence of the integrated galactic initial mass function depending on the star formation rate, leading to higher oxygen yield in systems where the star formation rate is high. More massive galaxies are expected to have higher yields and thus have a tendency to have higher metallicities. Dalcanton (2007) presented a series of closed-box chemical evolution models including infall and outflow. She has shown that neither simple infall nor outflow can reproduce the observed low effective yields in low-mass galaxies (see Lee et al. 2006 for a similar conclusion), but metal-enriched outflows can do. That is, effectively the freshly synthesized elements need to be removed from the matter cycle, which is, as noted by Köppen et al. (2007) in principle, equivalent to reducing the number of massive stars.**

Many recent studies in galaxy evolution trace changes in scaling relations of galaxies at earlier epochs. In this context, the galactic chemical abundances at different cosmic epochs can assist in constraining the likely scenarios of galaxy evolution. Different groups have used the classical nebular diagnostic techniques developed to study the properties of HII regions and emission line galaxies in the local universe to probe the properties of the interstellar gas in intermediate ($0 < z < 1$: Hammer et al. 2001; Lilly et al. 2003; Liang et al. 2006; Maier et al. 2004; Kobulnicky & Kewley 2004; Maier et al. 2005; Mouhcine et al. 2006ab; Lamareille et al. 2006) and high-redshift

galaxies ($1.5 < z < 4$: Pettini et al. 1998; Kobulnicky & Koo 2000; Mehlert et al. 2002; Lemoine-Busserolle et al. 2003; Erb et al. 2006; Maier et al. 2006). The oxygen abundances for the interstellar medium for luminous star-forming galaxies at intermediate redshift are found to cover the same range as their local counterparts, and most of them fall on the local luminosity-metallicity relation. However, a minority appear to have significantly lower oxygen abundances than the local galaxies with similar luminosities (Kobulnicky et al. 2003; Lilly et al. 2003; Liang et al. 2004; Mouhcine et al. 2006a). These luminous, massive, intermediate redshift, star-forming galaxies with low oxygen abundances have bluer colours than the higher metallicity ones, and exhibit physical conditions, i.e., emission line equivalent width and ionization state, very similar to those of the local faint and metal-poor star-forming galaxies (Mouhcine et al. 2006a; Maier et al. 2005). The intermediate redshift massive and large galaxies with low gas-phase oxygen abundances are most likely immature galaxies that will increase their metallicities and their stellar masses to the present epoch. The diversity of the properties of the massive and large galaxies at intermediate redshifts supports the scenario whereby galaxies are still assembling their baryonic content between $z \sim 1$ and $z = 0$ (Hammer et al. 2005). For a sample of mostly disk, intermediate redshift field and cluster galaxies, Mouhcine et al. (2006a) have shown that oxygen abundances do not correlate with either the maximum rotation velocity, i.e. a proxy of the total mass, or with the emission scale length size of the galaxy (see also Lilly et al. 2003). **Savaglio et al. (2005) have shown that the observed redshift evolution of the mass-metallicity relation could be well reproduced by a simple closed-box model where the star formation timescale is proportional to the galaxy total baryonic mass.**

As these observational data for more statistically significant samples of galaxies accumulate, numerical simulations become important to understand galaxy formation in the context of the currently favored hierarchical clustering scenario. To be compared with the observational data – which provides not only dynamical information, such as stellar and gas mass and rotation velocity, but also properties of stellar content, such as metallicity and age – such simulations are required to follow both the dynamical and chemical evolution of galaxies (e.g.: Mosconi et al. 2001; Lia et al. 2002; Kawata & Gibson 2003; Kobayashi et al. 2006). Using chemodynamical numerical simulations, we have built an ensemble of simulated late-type galaxies, spanning a factor of 50 in total mass, and sampling a range of assembly histories at a given total mass. We compare our large sample of simulated galaxies with recent observational results, and examine how the current simulations can explain the observations. We pay particular attention to the observed correlations between the galaxy mass and metallicity of both the gaseous and stellar components, key observables in disentangling the formation history of galaxies. In Section 2 we describe our numerical simula-

tions. Section 3 provides comparisons between simulated galaxies and observations. We summarize our conclusions in Section 4.

2. Simulations

The ensemble of simulated galaxies analysed here are patterned after the adiabatic feedback model of Brook et al. (2004), using the chemo-hydrodynamical evolution code **GCD+** (Kawata & Gibson 2003). The simulation models based on the semi-cosmological version of the code have been extensively used in our previous studies of galaxy properties. Brook et al. (2004) demonstrated that newly introduced adiabatic feedback model helps to create more realistic late-type disk galaxies. Brook et al. (2004; 2005) could reproduce the properties of both the thin and thick disk observed in the Milky Way and galaxies beyond the Local Group. Renda et al. (2005) used a part of the sample analysed here, to show that these simulated galaxies can reproduce the observed halo metallicities for galaxies with different masses. Details of both **GCD+** and the feedback model can be found elsewhere (Kawata & Gibson 2003; Brook et al. 2004; Renda et al. 2005), and we therefore only summarize briefly this information here.

The code is based on **TreeSPH** (Hernquist & Katz 1989; Katz, Weinberg & Hernquist 1996), which combines the tree algorithm (Barnes & Hut 1986) for the computation of the gravitational forces with the smoothed particle hydrodynamics (SPH) (Lucy 1977; Gingold & Monaghan 1977) approach to numerical hydrodynamics. The dynamics of the dark matter and stars is calculated by the N -body scheme, and the gas component is modeled using SPH. It is fully Lagrangian, three-dimensional, and highly adaptive in space and time owing to individual smoothing lengths and individual time steps. Moreover, it includes self-consistently almost all the important physical processes in galaxy formation, such as self-gravity, hydrodynamics, radiative cooling, star formation, supernova feedback and metal enrichment.

Radiative cooling is computed using a metallicity-dependent cooling function (derived with **MAPPINGSIII**: Sutherland & Dopita 1993). The cooling rate for solar metallicity gas is larger than that for gas of primordial composition by more than an order of magnitude. Thus, the cooling by metals should be accounted for in numerical simulations of galaxy formation. We use the following three criteria for star formation: (i) the gas density is greater than a critical density, $\rho_{\text{crit}} = 2 \times 10^{-25} \text{ g cm}^{-3}$, i.e. $n_{\text{H}} \sim 0.1 \text{ cm}^{-3}$; (ii) the gas velocity field is convergent, $\nabla \cdot \mathbf{v}_i < 0$; and (iii) the Jeans unstable condition, $h/c_s > t_g$, is satisfied, here h , c_s , and $t_g = \sqrt{3\pi/16G\rho_g}$ are the SPH smoothing length, the sound speed, and the dynamical time of the gas respectively. We used a fixed star formation efficiency independently of the halo mass. The effect of the ultraviolet background radiation field was not included.

We distribute the feedback energy from supernovae explosions in purely thermal form, although a fraction

of it could, in principle, be distributed in kinetic form. Following Brook et al. (2004), the energetic feedback is implemented such as the gas within the SPH smoothing kernel of Type II supernovae is prevented from cooling for the lifetime of the lowest mass star that ends as a Type II supernovae, i.e. the lifetime of an $8 M_{\odot}$ star (see also Thacker & Couchman 2000).

The metal enrichment was derived using supernovae Type II and Ia, and the mass loss from intermediate mass stars, relaxing the instantaneous recycling approximation. The code calculates the event rates of SNe II and SNe Ia, and the yields of SNe II, SNe Ia and intermediate mass stars for each star particle at every time step, considering the Salpeter (1955) initial mass function (mass range of 0.1 - $60 M_{\odot}$) and metallicity dependent stellar lifetimes. We assume that each massive star ($\geq 8 M_{\odot}$) explodes as a Type II supernova. The SNe Ia rates are calculated using the model proposed by Kobayashi, Tsujimoto & Nomoto (2000). The yields of SNe II, SNe Ia and intermediate mass stars are taken from Woosley & Weaver (1995), Iwamoto et al. (1999), and van den Hoek & Groenewegen (1997). The simulation follows the evolution of the abundances of several chemical elements (^1H , ^4He , ^{12}C , ^{14}N , ^{16}O , ^{20}Ne , ^{24}Mg , ^{28}Si , ^{56}Fe , and Z , where Z is the total metallicity).

For each model, we start with an isolated sphere of dark matter and gas, on to which small-scale density fluctuations based on a CDM power spectrum are superimposed using **COSMICS** (Bertschinger 1998). These fluctuations are the seeds for local collapse and subsequent star formation. The “top-hat” overdensity has an amplitude δ_i at initial redshift z_i , which is approximately related to the collapse redshift z_c by $z_c = 0.36\delta_i(1 + z_i) - 1$ (e.g. Padmanabhan 1993). Solid-body rotation corresponding to a spin parameter λ is imparted to the initial sphere to mimic the effects of longer wavelength fluctuations. As we focus here on the effect of the differences in galaxy assembly histories on galaxy properties, we fixed the collapse redshift and spin parameter. To guarantee that the end-product of the simulations would be disk-like system, we have chosen a high spin parameter (see also Brook et al. 2004; 2005). The relevant parameters include $\Omega_0 = 1$, baryon fraction $\Omega_b = 0.1$, $\sigma_8 = 0.5$, $H_0 = 50 \text{ km s}^{-1} \text{ Mpc}^{-1}$, the collapse redshift $z_c = 2$, and the spin parameter $\lambda = 0.060$.

A series of 112 simulations were generated using the same collapse redshift z_c , and spin parameter λ , for four different halo total masses, $M_{\text{tot}} = 10^{11} M_{\odot}$, $5 \times 10^{11} M_{\odot}$, $10^{12} M_{\odot}$, and $5 \times 10^{12} M_{\odot}$. We used 14147 dark matter and 14147 gas/star particles, for the ensemble of simulations analysed here. For each total mass, we run models with different patterns of initial small-scale density fluctuations which lead to different hierarchical assembly histories. This was controlled by setting different random seeds for the Gaussian perturbation generator in **COSMICS**.

In our main sample, both the collapse redshift and the spin parameter have been fixed in order to sample only the pattern of initial density perturbations, and thus the formation history. To investigate the properties of galaxies

which collapsed at a lower redshift, we also run a subset of 9 simulations with a total mass of $10^{11} M_{\odot}$, collapse redshift $z_c = 1.5$, and spin parameter $\lambda = 0.054$. Note that the definition of collapse redshift is for a spherical system with no rotation. If there is rotation, i.e., additional kinetic energy, the real collapse redshift would be lower and it is more complicated to be estimated. Therefore, we have chosen a lower spin parameter for this lower collapse model, to guarantee that the system collapses before $z=0$.

Admittedly, the semi-cosmological models are not fully self-consistent galaxy formation models, compared to the full-cosmological simulations (e.g.: Steinmetz & Navarro 1999; Abadi et al. 2003; Kawata et al. 2004; Bailin et al. 2005; Okamoto et al. 2005; Governato et al. 2006). As a benchmark for the semi-cosmological framework, we have also analysed the disc galaxy simulations from Bailin et al. (2005), which are fully cosmological within a Λ -dominated CDM cosmology (see Bailin et al. 2005 for details).

In the following, and for the ensemble of the simulated galaxies, the stellar mass is derived from the stars situated within 15 kpc of the centre of the stellar mass distribution, while the metallicity and the luminosity-weighted age of integrated stellar populations and the interstellar medium abundances are measured within 10 kpc of the centre. Stellar particles in the simulated galaxies represent simple stellar populations with a given age and metallicity. The photometric properties of the simulated galaxy stellar populations were estimated using the population synthesis models of Mouhcine & Lançon (2003), taking into account both the age and the metallicity of each stellar particle. Broad band optical properties have been converted into the SDSS photometric system as in Fukugita et al. (1996).

3. Results

3.1. Galaxy mass assembly

Figure 1 shows the evolution of star formation rates for all stars within $r = 15$ kpc at $z = 0$ as a function of redshift for the ensemble of galaxies in our synthetic sample. The figure shows that the star formation histories of our simulated galaxies are quite diverse. For massive galaxies, the star formation takes place continuously and smoothly. This is because the enhancement of the star formation due to the deeper potential and the existence of heavy elements (leading to rapid radiative cooling) is larger than the star formation suppression by thermal feedback (see Kawata & Gibson 2003 and Kobayashi et al. 2007 for similar analysis). For the majority of these galaxies, the star formation rates show peaks around $z \sim 1$ and then decline during later cosmic epochs. For low mass galaxies, the star formation histories show however striking differences. Due to their low metal content and shallower potential, the energy feedback from supernovae explosions suppresses more efficiently the star formation in low mass systems, leading to more bursting star formation histories.

Figure 2 shows the redshift evolution of the stellar mass (right panel), and the total mass (left panel), the

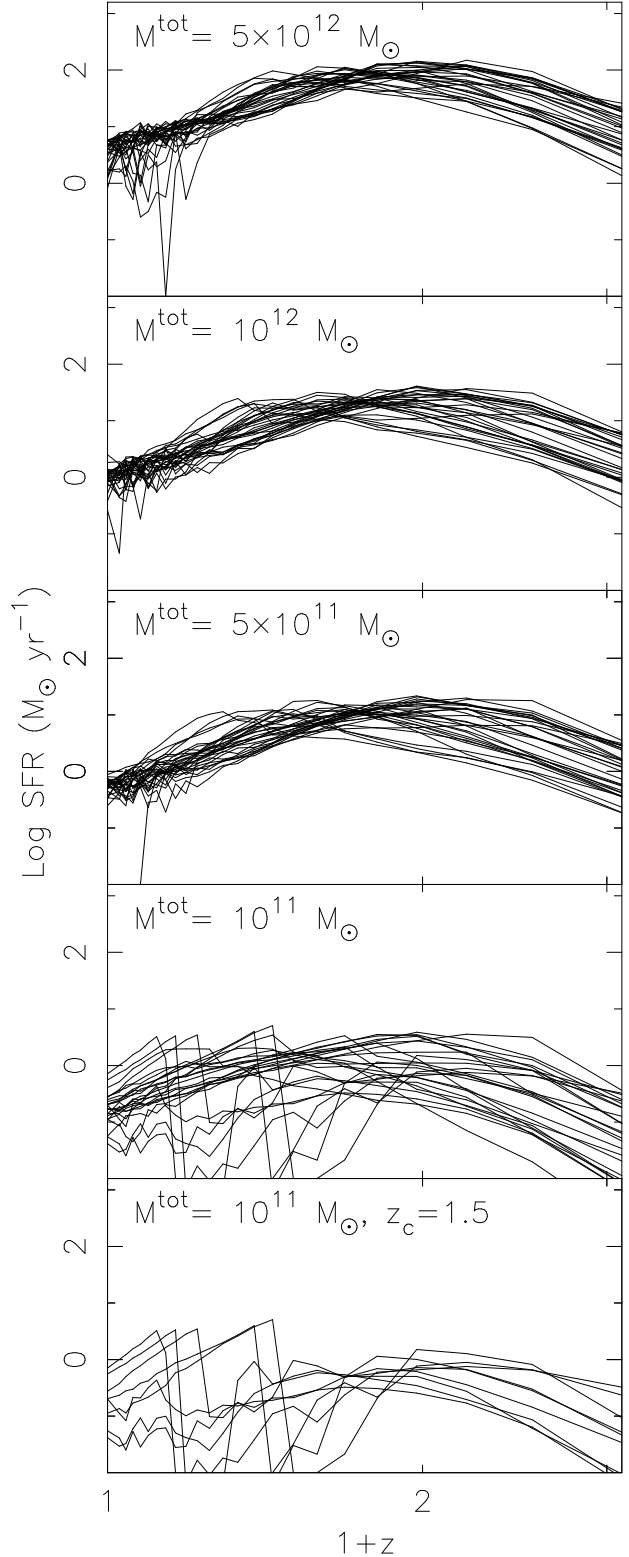


Fig. 1. Star formation rates as a function of redshift for the ensemble of galaxies analysed here.

latter including both dark and baryonic matter within the inner 100 kpc, normalized to their value at $z = 0$ for the ensemble of simulated galaxies ranked by their total mass. Solid black lines show the semi-cosmological runs, solid red lines the cosmological ones, and solid magenta lines

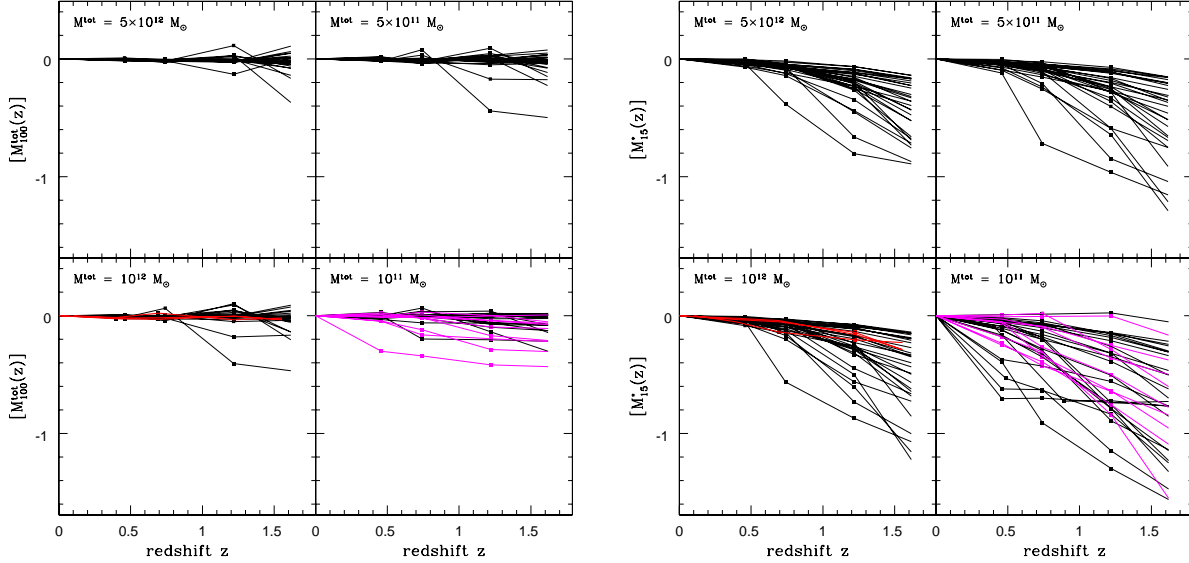


Fig. 2. Left: the redshift evolution of the total mass within the 100 kpc central region normalised to the $z = 0$ value for each subset. The semi-cosmological simulations with collapse redshift $z_c = 2$ are shown as black solid lines, those with collapse redshift $z_c = 1.5$ are shown in magenta. The cosmological simulations are shown in red. Right: similar to the left panel but for the stellar mass within the 15 kpc central region normalised to the $z = 0$ value.

the semi-cosmological simulations with collapse redshift $z_c = 1.5$. We note in passing that the assembly histories of both the total and the stellar mass in the semi-cosmological *and* the cosmological simulations are similar. The observed consistency is reassuring and leads us to conclude that the former are not affected significantly by not being fully cosmological.

The figure shows that the assembly of the total mass within the inner 100 kpc regions of galaxies is completed by $z \gtrsim 1.5$, independently of their total mass. On the other hand, the stellar mass in the central 15 kpc regions shows more extended assembly histories, with a large variety of assembly histories. While a fraction of the simulated galaxies have assembled their stellar content at early times, typically by $z \sim 1.5$, others continue to form stars to much later epochs. Galaxies with comparable stellar mass can have significantly different assembly histories of their stellar content, and diverse gaseous contents. As star formation does not proceed uniformly in all systems, galaxy stellar mass should not necessarily be considered a robust indicator of the merging history nor a good tracer of the total baryonic galaxy mass.

Fig. 3 shows the relationship between the total mass and the stellar mass of the galaxies in our simulated sample at different redshifts. The semi-cosmological simulations with collapse redshift $z_c = 2$ are shown as filled symbols, those with the collapse redshift $z_c = 1.5$ are shown as open boxes. The cosmological simulations are shown as open triangles. The predicted relationship is compared to the observed data in Böhm & Ziegler (2006) and Conselice et al. (2005), shown as four and six vertex stars, respectively. A correlation between the stellar and the total mass

is present from $z \sim 1$ to the present day. The galaxy stellar mass increases as a function of the mass of the host dark halo, in agreement with the observed correlation. The scatter in the model around the predicted relation increases with redshift. Galaxies with a total mass of $\sim 10^{11} M_\odot$ show a factor of ten variation in the stellar mass at all redshifts. At a given total mass, simulated galaxies with low stellar mass tend to be less evolved than those with more massive stellar contents. It is worth to mention that a tighter correlation is predicted between the total mass and the baryonic mass, where the latter span a more restricted range than the stellar mass. The predicted correlation is due to the fact that smaller systems tend to have a larger fraction of baryons in the form of gas at all redshifts (see below), in agreement with the results of De Rossi et al. (2007).

3.2. Gas-phase oxygen abundance vs. stellar mass

Our simulations follow the enrichment of individual chemical elements, so we estimate directly the gas-phase oxygen abundance as $12 + \log(\text{O}/\text{H})$. In Fig. 4 we show the relationship between stellar mass and oxygen abundance of gas particles for galaxies in our simulated sample at different cosmic epochs. Note that the results for the cosmological simulations broadly agree with the semi-cosmological ones in spite of the differences between the two frameworks (see Sect. 2).

The results at redshift $z = 0$ are compared to the observed local relation. The local sample used here is the sample of star-forming galaxies in the so-called “main galaxy sample” of the SDSS Data Release Four (Adelman-

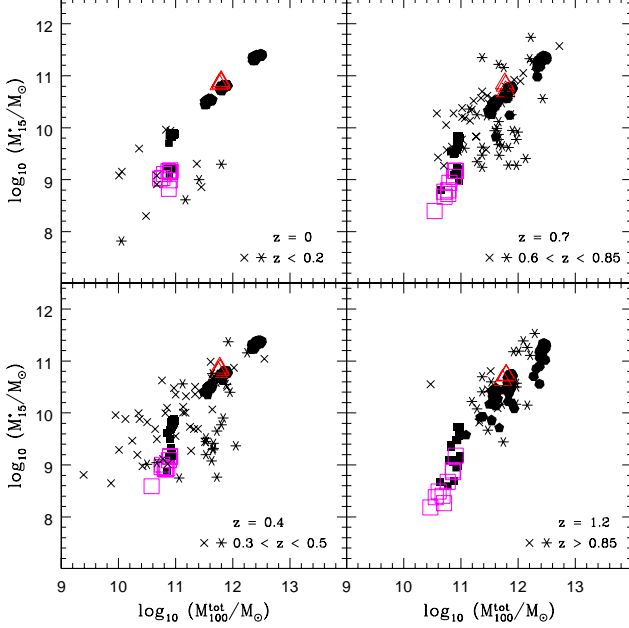


Fig. 3. The stellar mass against the total mass at different redshifts in our simulated sample. The semi-cosmological simulations with collapse redshift $z_c = 2$ are shown as filled symbols, those with collapse redshift $z_c = 1.5$ are shown as larger empty boxes. The cosmological simulations are shown as open triangles. The relationships for simulated galaxies are compared with the observed ones in Böhm & Ziegler (2006) and Conselice et al. (2005), shown as four and six vertices stars, respectively.

McCarthy et al. 2006). Gas-phase oxygen abundances are determined as described in Tremonti et al. (2004). At the present epoch, the predicted relationship between the stellar mass and the gas-phase oxygen abundance changes as a function of the galaxy stellar mass. For the galaxies with stellar masses larger than $\sim 10^{10} M_\odot$, the stellar mass-gas oxygen abundance relation is flat, with significant scatter, with solar abundances ($12 + \log(\text{O}/\text{H}) = 8.69$; Allende Prieto et al. 2001) or above, while galaxies with stellar masses lower than $\sim 10^{10} M_\odot$ show lower oxygen abundances, with a sharp transition between these two classes of galaxies. Massive galaxies with similar stellar masses show a range of gas-phase abundances, suggesting that stellar mass is not the only driver of the metallicity. The sharply separated population of metal-rich galaxies with stellar masses of $\sim 10^{10} M_\odot$ and metal poor galaxies with stellar masses of $\sim 10^9 M_\odot$ come from models with total masses of $M_{\text{tot}} = 10^{11} M_\odot$. The separation of the two population is due to the difference of the assembly history of galaxies, and the strong suppression of star formation in low mass systems to $z = 0$.

The results at $z = 0$ are in broad agreement with the local relation for star-forming galaxies. We would like to stress that we have not adjusted the absolute value of gas-phase oxygen abundance to the observed value, nor

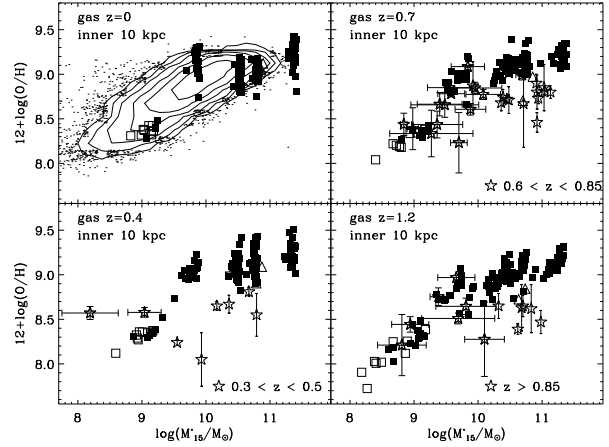


Fig. 4. The oxygen abundance of the gaseous component against the stellar mass, at different redshifts for simulated galaxies. The symbols are the same as in Fig. 3. The gas oxygen abundance predicted at the present epoch is compared with the relation obtained for a large sample of local SDSS late-type star-forming galaxies shown as small points and solid contours. The contours are spaced in number density with a factor of 2 between two consecutive contours. The results at intermediate redshifts are compared with the mass-oxygen abundance relationship in Savaglio et al. (2005) and Liang et al. (2006) shown as open stars.

have we fine-tuned the star formation efficiency to match the data. Therefore, it is encouraging that the absolute value of the oxygen abundances of the simulated galaxies at the present day is consistent with the observed ones. The predicted scatter of the gas-phase metallicity at a given galaxy stellar mass at $z = 0$ is similar to that observed for local galaxies in the SDSS.

As explained in Sect. 2, both the collapse redshift $z_c = 2$ and the spin parameter $\lambda = 0.06$ have been fixed in order to sample only the pattern of initial density perturbations, and thus the formation history, in the semi-cosmological framework. We have released this constraint on the subset at $M_{\text{tot}} = 10^{11} M_\odot$ and completed nine runs with collapse-redshift $z_c = 1.5$ and spin-parameter $\lambda = 0.054$. Fig. 4 shows that our sub-sample of $M_{\text{tot}} = 10^{11} M_\odot$ systems with $z_c = 1.5$ are broadly as evolved as the most metal-poor simulations at the same M_{tot} with collapse-redshift $z_c = 2$. This suggests that the feedback from supernovae more easily suppresses star formation in galaxies with lower collapse redshift, i.e. the galaxies formed from lower σ density perturbations.

Fig. 4 shows that the redshift evolution of the relationship between the stellar mass and the gas metallicity depends on the mass. For galaxies with stellar masses larger than $\sim 10^{10} M_\odot$, the level of chemical enrichment shows a modest change as a function of the redshift, as they have consumed large fractions of their gas reservoirs at high redshift. Their mass-metallicity relationship remains

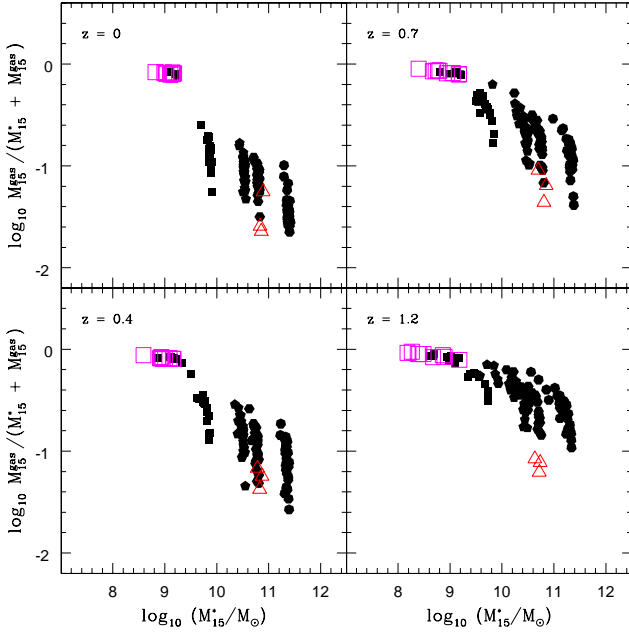


Fig. 5. The relationship between the gaseous fraction and the galaxy stellar mass at different redshifts. The symbols are the same as in Fig. 3.

nearly as flat as at the present epoch. As the universe ages, there is however a systematic enrichment of the metal content of the low stellar mass galaxies, together with the increase in their stellar contents by a large factor, migrating from stellar masses of $\sim 10^9 M_\odot$ to $\sim 10^{10} M_\odot$. Due to their extended star formation histories, masses and metallicities of low mass galaxies evolve more slowly than for their high mass counterparts. At all redshifts, the slope of the stellar mass-metallicity relation for low stellar mass galaxies tends to be steeper than the relation outlined by massive ones. The build up of the transition from the metal-rich and high stellar mass galaxies to the metal-poor and low stellar mass ones is clear at $z = 0.4$. The transition from high stellar mass, metal-rich galaxies to low stellar mass, metal-poor galaxies gets smoother at higher redshift.

The predicted stellar mass-metallicity relations at intermediate redshifts are in broad agreement with the observed ones between $0.4 \leq z \leq 1$ from Savaglio et al. (2005) and Liang et al. (2006). The observational data show hints of a flat stellar mass-metallicity relation for massive galaxies up to $z \sim 1$, and an increase of the gas-phase metallicity as a function of the stellar mass at lower stellar masses. The predicted gas-phase oxygen abundances for low stellar mass simulated galaxies agree nicely with the observed ones, however gas-phase oxygen abundances of simulated massive galaxies tend to be systematically higher than observed. The metallicity evolution found in our simulations for massive galaxies since $z \sim 1$ is slower than observed. A better agreement with observations seems to require a feedback mechanism to de-

lay the star formation to later epochs in massive galaxies in order to prevent those galaxies from enriching their gas to a high metallicity at high redshifts. Note however that (at least) part of the offset between observed and simulated gas-phase abundances for massive galaxies could be due to systematic errors affecting the empirical measurements. The procedure used to derive gas-phase metallicities for intermediate redshift galaxies, i.e., the strong line method in the absence of temperature-sensitive emission lines, has been suspected to involve systematic errors, especially at the high-metallicity end (e.g., Kennicutt et al. 2003; Bresolin et al. 2004). In addition, oxygen abundances estimated using different calibrations of the strong line method may differ by factors of up to ~ 4 (Ellison & Kewley 2005).

If the star formation efficiencies are mass-dependent, more massive galaxies convert larger fractions of their gas into stars than low mass counterparts, and then have shorter timescale for their chemical evolution; therefore this could lead to the observed trend between stellar mass and gas-phase oxygen abundance. Fig. 5 shows the relationship between the baryonic gas fraction – i.e., the ratio between the gaseous mass and the baryonic mass – and the stellar mass at different redshifts. In our simulations, the baryonic gas fraction correlates with the stellar mass, in agreement with the observations of the local disc galaxies (e.g. Rosenberg et al. 2005). Low mass galaxies have larger gas fraction, implying that they have converted lower fractions of their interstellar gas into stars than galaxies with higher mass, and they are less chemically enriched. Even though a trend is present, which gets shallower at higher redshifts, galaxies of a given stellar mass span a wide range of gaseous-to-stellar mass ratio as a consequence of the large variety of their assembly histories. Note that the cosmological simulations tend to have low gas fraction. This can be traced to not having adopted the strong supernova feedback model of Brook et al. (2004), but adopting pure thermal feedback in these simulations. The weak feedback leads to more efficient consumption of the gas component, and their gas fraction remains low.

Our results agree with recent investigations that have attempted to place the stellar mass versus metallicity relation into an hierarchical context, using numerical simulations. De Rossi et al. (2007) used cosmological hydrodynamical simulations to reproduce roughly the local relation as a consequence of the variation of star formation efficiency with stellar mass. Similarly, Brooks et al. (2007) argue that galaxy mass loss does not directly suppress the metallicities of low mass galaxies, but that supernova feedback leads to low star formation efficiencies in those galaxies, which leads to low chemical abundances. Using high resolution cosmological simulations of high redshift galaxies, Tassis et al. (2006) have found that gas outflows escaping the host galaxy halo are not required to explain the observed scaling relations of dwarf galaxies. Again, scaling relations in simulated galaxies similar to those observed arise due to increasingly inefficient conversion of gas into stars in low mass galaxies rather than outflows.

Finlator & Davé (2007) have compared the observed stellar mass versus metallicity relation of star forming galaxies at $z \approx 2$ from Erb et al. (2006) with predictions from cosmological hydrodynamical simulations to argue however that outflows are required not only to suppress star formation but also to lower galaxy metal content. They claim that a feedback model where the outflow velocity scales as the escape velocity is necessary to reproduce the slope and normalization of the observed relation at $z \approx 2$. In this scenario, the scatter in the relation is due primarily to the dilution timescale, representing the timescale for a galaxy to return to an equilibrium metallicity (reflecting the enrichment balance between star formation and gas accretion) after a metallicity-perturbing interaction, compared to the dynamical timescale. However a potential concern here is that (i) the metallicity indicator used by Erb et al. (2006) may saturate for high metallicity galaxies, and (ii) the calibration used by those authors may underestimate oxygen abundances (see Liang et al. 2006 and Kennicutt et al. 2003 for more details). The normalization of the observed relation at $z \approx 2$ is still uncertain (see Erb et al. 2006 for more details). Interestingly, the slope of the stellar mass vs. metallicity relation predicted in their no-wind case is in fair agreement with observations, although simulated galaxies have higher abundances at a given stellar mass than estimated observationally. Finlator & Davé (2007) have not followed their simulations to the present epoch, where the observed stellar mass - metallicity relation is much less affected by systematic effects.

3.3. Stellar metallicity/age vs. stellar mass

Ages and metallicities of stellar populations are powerful tracers of galaxy star formation and chemical enrichment histories, and offer a way of constraining their assembly histories. Fig. 6 shows the relationship between the V-band luminosity-weighted total metallicity and the integrated stellar mass at different redshifts. The results at redshift $z = 0$ are compared to the observed local relation. The local sample used here was selected from the “main galaxy sample” of the SDSS Data Release Four. The models presented here are designed for late-type galaxies. For a meaningful comparison, we have split this sample into nominally early and late-type galaxies. The (inverse) concentration index, defined as the ratio of the radii enclosing 50% (R_{50}) and 90% (R_{90}) of the Petrosian r -band galaxy light, is used as a proxy for galaxy morphology indicator (Shimasaku et al. 2001; Strateva et al. 2001). Baldry et al. (2006) have found that a concentration index around ~ 0.4 is a natural dividing line between red and blue galaxy populations for all stellar masses. We selected late-type galaxies from the “main galaxy sample” by selecting galaxies with concentration index greater than 0.4. Stellar metallicities are determined as described in Gallazzi et al. (2005). The predicted relationship between the luminosity-weighted stellar metallicity and the

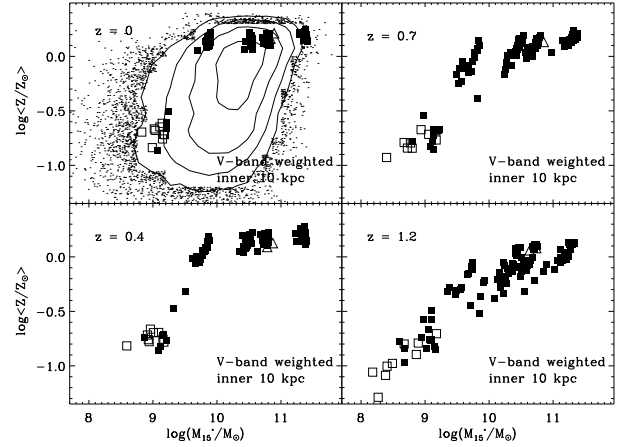


Fig. 6. The V-band luminosity-weighted mean total metallicity of the integrated stellar populations against the integrated stellar mass, at different cosmic epochs. The symbols are the same as in Fig. 3. The results at $z = 0$ are compared with the relation between the stellar mass and the total metallicity of local late-type galaxies in the SDSS shown as a solid contours and small points. The contours are spaced in number density with a factor of 2 between two consecutive contours. See the text for more details.

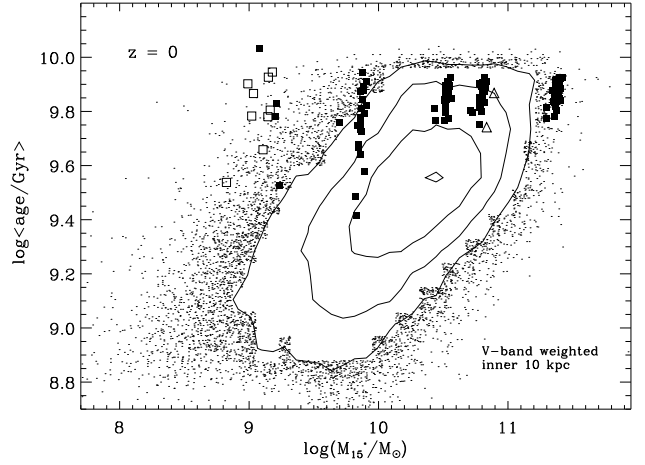


Fig. 8. The V-band luminosity-weighted mean age for the integrated stellar populations, against the stellar mass at redshift $z = 0$. The symbols are the same as in Fig. 3. The results are compared with the relation between the stellar mass and the age of local late-type galaxies in the SDSS. The contours are spaced in number density with a factor of 2 between two consecutive contours.

integrated stellar mass at the present epoch is in broad agreement with the observed local relation for late-type galaxies over ~ 3 orders of magnitude in stellar mass.

The general behaviour of the predicted relationship between stellar metallicity and stellar mass at the different redshifts is similar to the evolution of the relation for the gas-phase oxygen abundance, with the predicted

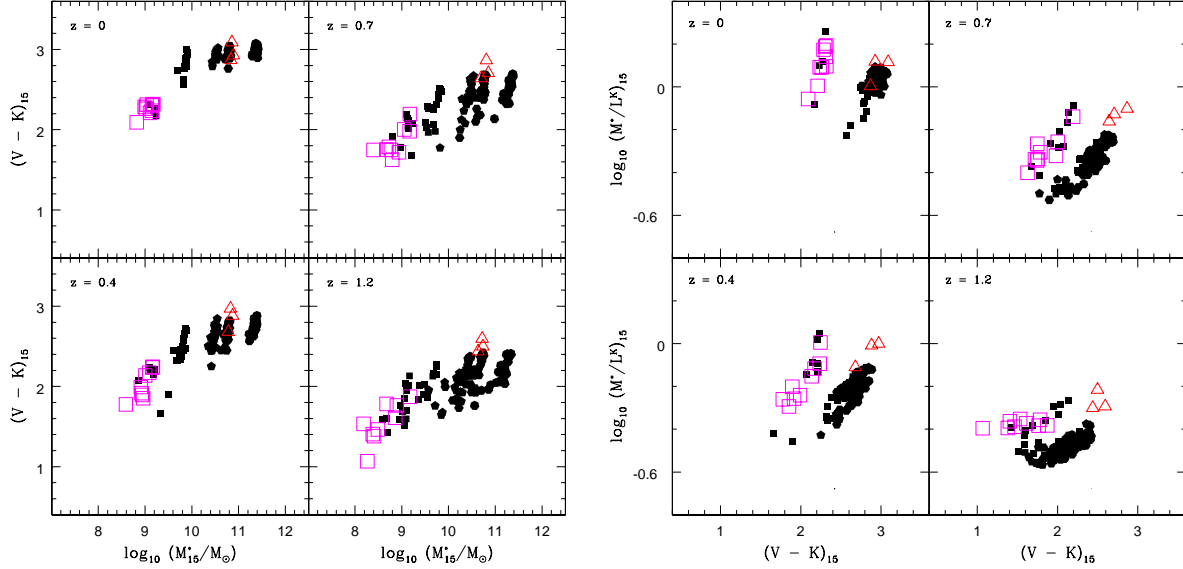


Fig. 7. The relationships between the integrated stellar population (V-K) colour and the stellar mass (left panel) and the K-band stellar mass-to-light ratio (right panel) in our simulated sample at different redshifts. The symbols are the same as in Fig. 3.

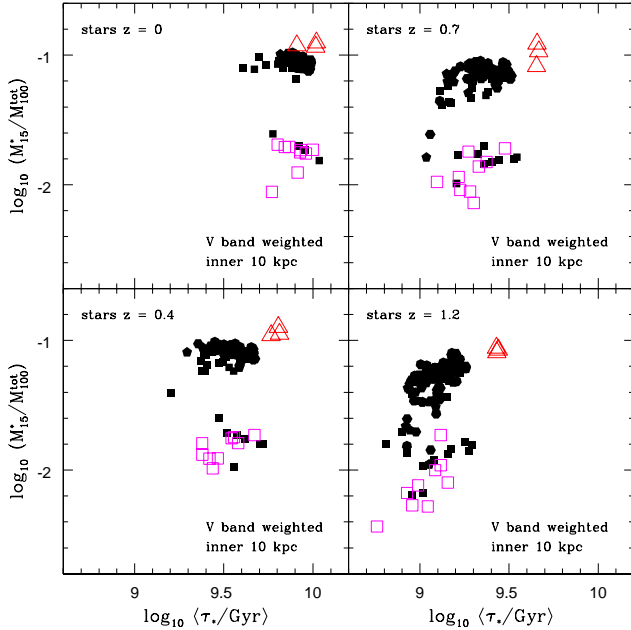


Fig. 9. The stellar-to-total mass ratio against the V-band luminosity-weighted mean age for the integrated stellar populations. The symbols are the same as in Fig. 3.

stellar metallicities less dispersed than the gas-phase oxygen abundances at a given galaxy stellar mass. The predicted local relationship shows a transition from massive galaxies, with a flat metallicity-mass relation, to low stellar mass galaxies, with a steeper relation. The redshift evolution of the stellar metallicity-mass relation is mainly driven by the low mass systems, in agreement with the

results of De Rossi et al. (2007) who found that systems with stellar masses smaller than a few times $\sim 10^{10} M_{\odot}$ are responsible for the evolution of this relation at least from $z \approx 3$. Massive galaxies in the simulations assembled their stars earlier (see Fig. 2), making the relation steeper for low mass systems than for their massive counterparts.

The left panel of Fig. 7 shows the relationship between the integrated stellar population (V-K) colour and the stellar mass. The colours are estimated using the luminosities of the integrated stellar populations within the central regions of simulated galaxies. Red galaxies in the simulated sample are predominantly massive, in agreement with observations (e.g., Borch et al. 2006), as the most massive simulated galaxies have the most metal-rich stellar populations (see below). The relationship between integrated stellar population colours and stellar mass is present up to $z \sim 1$, although the scatter in the correlation is more substantial at earlier cosmic epochs. For present-day galaxies in our simulated sample, the (V-K) colours seem to flatten at stellar masses $\sim 10^{10} > M_{\odot}$. This flattening gets weaker at higher redshifts.

The fraction of the baryonic mass converted from gas into stars in the simulated galaxies (not shown here) is found to correlate with the stellar population colours at all redshifts – i.e. gas rich galaxies are on average the bluer ones, in agreement with the observed local correlation between the atomic gaseous-to-stellar mass ratio and the optical/near-infrared colour (Kannappan et al. 2004; see also Geha et al. 2006). The relationship is driven by the correlation between the baryonic gas fraction and the stellar metallicity, in agreement with that inferred from the observed correlation between the metallicity-sensitive near-infrared colour and the gaseous mass fraction (Galaz

et al. 2002). This also implies that the lower level of chemical evolution of the stellar component of low mass galaxies is primarily due to their low efficiency at converting gas into stars, as discussed above.

The right panel of Fig. 7 shows the relationship between the K-band stellar mass-to-light ratio and the integrated stellar population (V-K) colour. Although with a large scatter, galaxies with low stellar mass and high baryonic gas fraction, tend to have lower mass-to-light ratio and bluer colours than those with high stellar mass and low gaseous fraction, in agreement with recent observational results (Galaz et al. 2002). We also found that the mass of the gaseous component in the simulated galaxies does not correlate with the stellar mass-to-light ratio in agreement with observations of local disc galaxies (Rosenberg et al. 2005). The relationship between integrated stellar population colour and stellar mass-to-light ratio is present up to $z \sim 1$, getting shallower at high redshift. The predicted correlation between the stellar mass-to-light ratio and colour is consistent with the suggestion that the stellar mass-to-light ratio varies along the Tully-Fisher relation (McGaugh & de Blok 1997). The figure illustrates that galaxies with a given stellar mass-to-light ratio span a large range of integrated stellar population colours. Each of the two parallel sequences in the mass-to-light ratio versus colour diagram are populated by galaxies with comparable stellar and gas-phase metallicities, but their luminosity-weighted ages range from ~ 3 to ~ 10 Gyr (see below).

Fig. 8 shows the $z = 0$ relationship between the stellar mass and the V-band luminosity weighted mean age of integrated stellar populations for our sample of simulated galaxies. The predictions are compared to the relationship derived for the local late-type galaxies selected from the SDSS Data Release Four. We find no relation between the luminosity weighted ages and the stellar mass. Large galaxies with stellar masses larger than $\sim 10^{10} M_{\odot}$ have ages ranging from 6 Gyr to 9 Gyr, in agreement with the ages of SDSS galaxies with similar stellar masses. For low stellar mass galaxies in our simulated sample, the mean ages are more dispersed than for the massive ones, ranging from ~ 3 to ~ 10 Gyr, older than what is estimated for local galaxies.

Fig. 9 shows the relationship between the age and the ratio of the integrated stellar mass to the total mass, the latter including both dark and baryonic matter within the inner 100 kpc, at different redshifts. As shown in Fig. 2 the total mass in the inner 100 kpc does not change substantially since $z \sim 1.5$, and the predicted redshift evolution of the stellar-to-total mass ratio is driven mainly by the variation of the stellar mass. At all redshifts, while the stellar-to-total mass ratio covers a wide range, the integrated stellar populations tend to be dominated by similarly old stars independently of galaxy stellar and/or total mass. Erb et al. (2006) have suspected the presence of a correlation between the galaxy dynamical-to-stellar mass ratio and the stellar population age at $z \sim 2$. From the Erb et al. (2006) data (see their Fig. 7), it seems that galax-

ies with low stellar mass tend to have large dynamical-to-stellar mass ratio, indicating that those galaxies have recently begun forming stars. The so-called downsizing, in which the stellar mass of the galaxies undergoing active star formation become progressively lower as later epochs (Cowie et al 1996), is not seen in our simulations, i.e., there are insufficient numbers of younger stellar populations in galaxies with low stellar masses in our simulations (see also Kobayashi et al. 2006 for a similar conclusion). This age problem, as outlined above, signals two problems in our simulations. First, there is an excess of old galaxies with stellar masses of $\sim 10^{10} M_{\odot}$. They correspond to galaxies that show high metallicity already at high redshift as seen in Fig. 6. At the present epoch, they are dominated by old and metal rich stellar populations. Their star formation should be more suppressed at high redshift, and more self-regulated since $z \sim 1$. The feedback from supernovae should be more effective for these galaxies, preventing gas from collapsing and cooling in the early stage of the hierarchy, in order to ensure that most of the stellar content of galaxies does not form early. This has already been recognised and invoked in previous numerical studies of the angular momentum of galaxies (e.g.: Weil et al. 1998; Steinmetz & Navarro 1999; Sommer-Larsen et al. 2003). Second, galaxies with stellar masses of $\sim 10^9 M_{\odot}$ are too old. This is due to an overly strong suppression of star formation for these galaxies. These galaxies form very few stars at the present epoch, and are dominated by old stars. Note that the luminosity-weighted stellar metallicities for these galaxies are consistent with the observed ones at $z = 0$ (Fig. 6). Their gas-phase metallicity is low (Fig. 4), because there is an excess of gas remaining at the present epoch. Solving this problem requires a mechanism which maintains a moderate amount of star formation since $z \sim 1$, and blows out a fraction of the gas or suppresses the gas infall. A combination of stronger supernovae feedback and the UV background radiation (e.g., Efstathiou 1992) may help to solve this problem. Alternatively, a mass-dependence of the star formation efficiency could also help to alleviate the age problem.

3.4. The Colour-Magnitude Relation

To illustrate a further signature of what is likely to be a problem for our simulated sample, Fig. 10 shows the relationship between the $(g-r)$ colour and the i -band luminosity for the simulated galaxies at the present epoch, compared to the observed relation for a sample of disc-dominated galaxies, selected by Pizagno et al. (2004) from the SDSS with a disc-to-total luminosity ratio larger than 0.9, shown as empty squares. The other symbols are the same as in Fig. 3. Since we have not applied any treatment for internal extinction in our simulations, we have compared the predicted colour-magnitude relation to the sample of Pizagno et al. (2004) for which the internal dust reddening was corrected for as in Tully et al. (1998), rather than to the low redshift New York University Value-Added

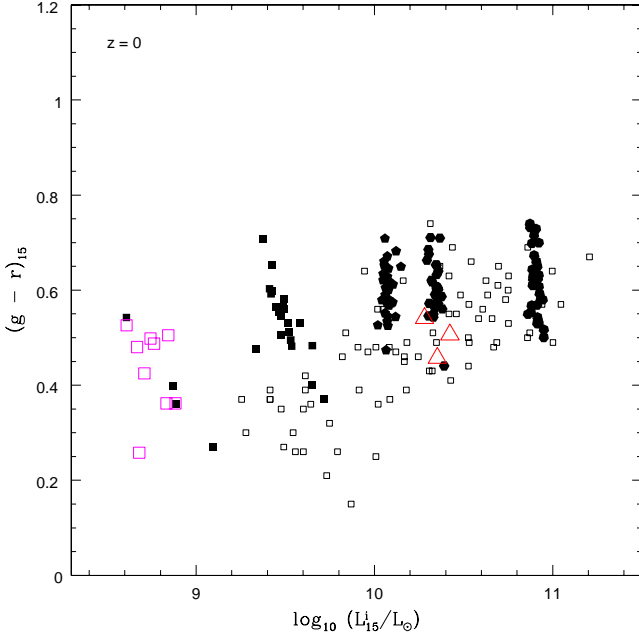


Fig. 10. The Colour-Magnitude relation for the simulated galaxies at $z = 0$. The symbols are the same as in Fig. 3. The predicted Colour-Magnitude relation is compared with the observed relation for a sample of local disc-dominated galaxies selected from the SDSS Pizagno et al. (2005), shown as empty small boxes.

Galaxy Catalogue (Blanton et al. 2005) for which magnitudes are not extinction-corrected.

The integrated colour of local late-type galaxies is correlated with the absolute luminosity, in the sense that bright late-type galaxies tend to be redder than the faint ones (e.g. Tully et al. 1982; Bothun et al. 1984; Peletier & de Grijs 1998). The colours of simulated luminous galaxies are in agreement with observed ones, as a consequence of the agreement between predicted and observed ages and stellar metallicities of massive galaxies. The scatter of the integrated colours of simulated galaxies, reflecting the differing formation histories which have been sampled, agrees with the observed scatter for the disc-dominated galaxy colours. Since it is difficult to assign morphological types to galaxy models, our simulated galaxy sample cannot be trimmed of galaxies morphologically earlier than those selected by Pizagno et al. (2005). With this caveat, we conclude that the colours and the scatter of bright galaxies in the simulated colour-magnitude relation are in agreement with observations.

Although the predicted colour scatter for the low stellar mass simulated galaxies is comparable to what is observed, faint galaxies in our simulated sample show redder integrated $(g - r)$ colours than observed for galaxies with similar luminosities, i.e. the simulated colour-magnitude relation is shallower than observed. The difference between the observed and the simulated integrated stellar population colours for faint galaxies is mainly driven by

the differences among the mean ages of the stellar populations (Fig. 6). Again, a mechanism to self-regulate the star formation in low mass galaxies to later epochs seems necessary to alleviate the discrepancy between the measured and the predicted stellar population ages and the colour-magnitude relation. The agreement found between simulated and observed stellar and gaseous metallicities at the present epoch, and at earlier cosmic epochs for low mass galaxies, suggests that the rate at which stars form in simulated galaxies might not be dramatically different from what it should be.

4. Summary

We have presented an analysis of the chemical properties over the last half of the age of the Universe for a sample of 112 simulated late-type galaxies, with stellar masses larger than $\sim 10^9 M_\odot$, formed under the hierarchical clustering scenario. The simulations include hydrodynamics, star formation, metal-dependent cooling, supernova feedback, and a chemical enrichment of the interstellar medium that relaxes the instantaneous recycling approximation. Stellar feedback is taken into account by injecting energy into the gas that surrounds regions of recent star formation. We compared the observed properties of the simulated galaxies with the recent observational data at various redshifts. A particular emphasis has been placed upon the relationship between the stellar mass and the metallicity of both the gaseous and the stellar components. The main results can be summarised as follows.

- In the hierarchical clustering scenario, even after the system has collapsed, the histories of the growth of the stellar mass in the central region can be different (Fig. 2) due to the variety in the minor merger and gas fueling histories, which also leads to the diverse fraction of the gas-to-stellar mass ratio among the galaxies with similar stellar or total mass (Fig. 5).
- The stellar mass in the inner region correlates well with the total mass of galaxies up to $z \sim 1.2$ (Fig. 3), which broadly agrees with the observed relation, especially for higher mass ($M_{\text{tot}} > 10^{10} M_\odot$) galaxies. Lower mass galaxies have greater scatter. For some simulated galaxies, star formation is heavily suppressed and leads to lower stellar mass compared with the total mass.
- We have analyzed the metallicity for both stellar and gas components. Both are correlated with the stellar mass up to $z \sim 1.2$, and show an agreement with recent observations (Figs. 4 and 6). This relation arises from the fact that higher mass galaxies convert gas more efficiently into stars.
- Higher mass galaxies reach a high metallicity earlier. As a result, the slope of the mass-metallicity relation becomes flatter with decreasing redshift (Figs. 4 and 6). Lower mass galaxies ($M_{\text{tot}} < 10^{10} M_\odot$) evolve chemically more slowly, and have lower metallicity than that predicted from the extrapolation of the mass-metallicity relation for higher mass galaxies at

lower redshifts, which is also consistent with the observational data.

- The predicted scatter in the mass-metallicity relation also reproduces qualitatively the observed scatter (Figs. 4 and 6). This suggests that the observed scatter could be due to the difference in mass assembly histories, a natural prediction of the hierarchical clustering scenario (Fig. 2).

The primary disagreement between our simulations and observations is as follows:

- Our simulations predict almost no correlation between the stellar age and the stellar mass, which cannot explain the observed significantly younger population in lower mass galaxies, e.g. stellar masses lower than $\sim 10^9 M_\odot$ (Fig. 8). As a result, the simulations also predict too flat of a colour-luminosity relation (Fig. 10).

This suggests that the simulations need a mechanism to sustain a low level of star formation activity and also keep the stellar and gas metallicity low. A combination of stronger supernovae feedback and the UV background radiation may help to cause such self-regulated star formation in the lower mass galaxies. This demonstrates that the quantitative comparisons made in the paper are invaluable to improve numerical simulation models, which eventually will aid in completing our understanding of the physical processes governing galaxy formation and evolution.

Acknowledgements. We acknowledge the Center for Computational Astrophysics, CfCA, of the National Astronomical Observatory, Japan (VPP5000 was used), the Institute of Space and Astronautical Science of Japan Aerospace Exploration Agency, and the Australian Partnerships for Advanced Computing, the Swinburne Supercomputer Facility support team, and the Commonwealth Cosmology Initiative. AR thanks Michael Blanton for helpful discussions, and the Liverpool John Moores University Astrophysics Research Institute, the University of Central Lancashire Centre for Astrophysics, and the Osservatorio Astronomico di Palermo for their kind hospitality. DK acknowledges the KITP NSF grant, PHY05-51164.

References

- Adelman-McCarthy J. K., et al., 2006, ApJS, 162, 38
- Allende Prieto C., Lambert D. L., Asplund M., 2001, ApJ, 556, L63
- Bailin J., Kawata D., Gibson B. K., et al., 2005, ApJ, 627, L17
- Barnes J.E., Hut P., 1986, Nature, 324, 446
- Bertschinger E., 1998, ARA&A, 36, 599
- Blanton M.R., Schlegel D.J., Strauss M.A., et al., 2005, AJ, 129, 2562
- Bothun G.D., Romanishin W., Strom S.E., Strom K.M., 1984, AJ, 89, 1300
- Bresolin F., Garnett D.R., Kennicutt R.C., 2004, ApJ, 615, 228
- Brodie J., Huchra J.P., 1991, ApJ, 379, 157
- Brook C.B., Kawata D., Gibson B.K., Flynn C., 2004, MNRAS, 349, 52
- Brook C.B., Gibson B.K., Kawata D., Martel H., 2005, ApJ, 630, 298
- Brooks A. M., Governato F., Booth C. M., Willman B., Gardner J. P., Wadsley J., Stinson G., Quinn T., 2007, ApJ Letters, 655, 17
- Böhm A., Ziegler B.L., 2006, submitted (astro-ph/0601505)
- Conselice C.J., Bundy K., Ellis R.S., Brinchmann J., Vogt N.P., Phillips A.C., 2005, ApJ, 628, 160
- Cowie L. L., Songaila A., Hu E. M., Cohen J. G., 1996, AJ, 112, 650
- Dalcanton, J. J., 2007, ApJ, 658, 941
- De Rossi M.E., Tissera P.B., Scannapieco C., 2005, MNRAS, 374, 323
- Efstathiou G., 1992, MNRAS, 256, 477
- Ellison S. L., & Kewley L. J., 2005, in "The Fabulous Destiny of Galaxies; Bridging the Past and Present (astro-ph/0508627)
- Erb D.K., Steidel C. C., Shapley A. E., Pettini M., Reedy N. A., Adelberger K. L., 2006, ApJ, 644, 813
- Finlator K., Davé R., 2007, MNRAS, submitted (astro-ph/07043100)
- Fukugita M., Ichikawa T., Gunn J.E., Doi M., Shimasaku K., Schneider D.P., 1996, AJ, 111, 1748
- Gallazzi A., Charlot S., Brinchmann J., White S.D.M., Tremonti C.A., 2005, MNRAS, 362, 41
- Garnett D.R., Shield G.A., 1987, ApJ, 317, 82
- Garnett D.R., Shield G.A., Skillman E.D., et al., 1997, ApJ, 489, 63
- Gingold R.A., Monaghan J.J., 1977, MNRAS, 181, 375
- Hammer F., Gruel N., Thuan T.X., Flores H., Infante L., 2001, ApJ, 550, 570
- Hammer F., Flores H., Elbaz D., Zheng X.Z., Liang Y.C., Cesarsky C., 2005, A&A, 430, 115
- Hernquist L., Katz N., 1989, ApJS, 70, 419
- Kannappan S. J., ApJ, 2004, 611, L81
- Katz N., Weinberg D.H., Hernquist L., 1996, ApJS, 105, 19
- Kawata D., Gibson B.K., 2003, MNRAS, 340, 908
- Kennicutt R.C., Jr., Bresolin F., Garnett D.R., 2003, ApJ, 591, 801
- Kobayashi C., Tsujimoto T., Nomoto K., 2000, ApJ, 539, 26
- Kobayashi C., Springel V., White S. D. M., 2007, MNRAS, 376, 1465
- Kobulnicky H. A., Koo D.C., 2000, ApJ, 545, 712
- Kobulnicky H.A., Willmer C.N.A., Phillips A.C., et al. 2003, ApJ, 599, 1006
- Kobulnicky H. A., & Kewley L. J., 2004, ApJ, 617, 240
- Köppen J., Weidner C., Kroupa P., 2007, MNRAS, 375, 673
- Lamareille F., Mouhcine M., Contini T., Lewis I. J., Maddox S. J., 2004, MNRAS, 350, 396
- Lamareille F., Contini T., Brinchmann J., Le Borgne J.-F., Charlot S., Richard J., 2006, MNRAS, 448, 907
- Lee H., Skillman E. D., Cannon J. M., Jackson D. C., Gehrz R. D., Polonski E. F., Woodward C. E., 2006, ApJ, 647, 970
- Lequeux J., Peimbert M., Rayo J.F., et al., 1979, A&A, 80, 155
- Lemoine-Busserolle M., Contini T., Pello R., Le Borgne J.-F., Kneib J.-P., Lidman C., 2003, A&A, 397, 839
- Lia C., Portinari L., Carraro G., 2002, MNRAS, 330, 821
- Liang Y.C., Hammer F., Flores H., Elbaz D., Marcellac D., Cesarsky C.J., 2004, A&A, 423, 867
- Liang Y.C., Hammer F., Flores H., 2006, A&A, 447, 113
- Lilly S.J., Carollo C.M., Stockton A.N., 2003, ApJ, 597, 730

- Lucy L.B., 1977, *AJ*, 82, 1013
- Maier C., Meisenheimer K., Hippelein H., 2004, *A&A*, 418, 475
- Maier C., Lilly S.J., Carollo M., Stockton A., Brodwin M., 2005, *ApJ*, 634, 849
- Maier C., Lilly S.J., Carollo M., Meisenheimer K., Hippelein H., Stockton A., 2006, *ApJ*, 639, 858
- Mateo M., 1998, *ARA&A*, 36, 435
- Mehlert D., Noll S., Appenzeller I., et al., 2002, *A&A*, 393, 809
- Mosconi M. B., Tissera P. B., Lambas D. G., Cora S. A., 2001, *MNRAS*, 325, 34
- Mouhcine M., Lançon A., 2003, *A&A*, 402, 425
- Mouhcine M., Bamford S.P., Aragon-Salamanca A., Nakamura O., Milvang-Jensen B., 2006a, *MNRAS*, 69, 891
- Mouhcine M., Bamford S.P., Aragon-Salamanca A., Nakamura O., Milvang-Jensen B., 2006b, *MNRAS*, 368, 1871
- Moustakas J., & Kennicutt R. C., 2006, *ApJ*, 651, 155
- Padmanabhan T., 1993, *Structure formation in the universe*, Cambridge University Press, Cambridge, UK
- Peletier R.F., de Grijs R., 1998, *MNRAS*, 300, L3
- Pettini M., Kellogg M., Steidel C.C., Dickinson M., Adelberger K.L., Giavalisco M., 1998, *ApJ*, 508, 539
- Pilyugin L. S., Ferrini F., 2000, *A&A*, 358, 72
- Pizagno J., Prada F., Weinberg D.H., et al., 2005, *ApJ*, 633, 844
- Richer M.G., McCall M.L., 1995, *ApJ*, 445, 642
- Renda A., Gibson B. K., Mouhcine M., Ibata R. A., Kawata D., Flynn C., Brook C. B., 2005, *MNRAS*, 363, 16
- Savaglio S., Glazebrook K., Le Borgne D., et al., 2005, *ApJ*, 635, 260
- Skillman E.D., Kennicutt R.C., Hodge P.W., 1989, *ApJ*, 347, 875
- Sommer-Larsen J., Götz M., Portinari L., 2003, *ApJ*, 596, 47
- Steinmetz M., & Navarro J. F., 1999, *ApJ*, 513, 555
- Strauss M. A., et al., 2002, *AJ*, 124, 1810
- Sutherland R.S., Dopita M.A., 1993, *ApJS*, 88, 253
- Tassis K., Kravtsov A. V., Gnedin N. Y., 2006, *ApJ*, submitted (astroph/0609763)
- Thacker R. J., Couchman H. M. P., 2000, *ApJ*, 545, 728
- Tremonti C.A., Heckman T.M., Kauffmann G., et al., 2004, *ApJ*, 613, 898
- Tully B.R., Mould J.R., Aaronson M., 1982, *ApJ*, 257, 527
- Tully R.B., Pierce M.J., Huang J.-S., Saunders W., Verheijen M.A.W., Witchalls P.L., 1998, *AJ*, 115, 2264
- Vilchez J.M., 1995, *AJ*, 110, 1090
- Weil M. L., Eke V. R., Efstathiou G., 1998, *MNRAS*, 300, 773
- Zaritsky D., Kennicutt R.C., Huchra J.P., 1994, *ApJ*, 420, 87